Space Dynamics Lab Publications   Space Dynamics Lab

Characterization of Particulate Emission from Animal Feeding Operations with Three-wavelength Lidar Using Simultaneous In-Situ Point Measurements as Calibration Reference Sources

Vladimir V. Zavyalov

Gail E. Bingham

Thomas D. Wilkerson

Jason Swasey

Christian Marchant

Christopher Rogers

See next page for additional authors

Follow this and additional works at: https://digitalcommons.usu.edu/sdl_pubs

Recommended Citation

Utah State University
MERRILL-CAZIER LIBRARY

Authors

Vladimir V. Zavyalov, Gail E. Bingham, Thomas D. Wilkerson, Jason Swasey, Christian Marchant, Christopher Rogers, Randy Martin, Phil Silva, and Vishal Doshi

Characterization of Particulate Emission from Animal Feeding Operations with Three-wavelength Lidar Using Simultaneous In-situ Point Measurements as Calibration Reference Sources

Vladimir V. Zavyalov[1,] Gail E. Bingham[1], Thomas D. Wilkerson[1], Jason Swasey[1], Christian Marchant[1], Christopher Rogers[1], Randy Martin[2], Phil Silva[2], and Vishal Doshi[2]

[1]Space Dynamics Laboratory, 1695 North Research Parkway, North Logan, UT 84341
Tel: 435-797-4116   Fax: 435-797-4599 vladimir.zavyalov@sdl.usu.edu
[2]Utah State University, Logan, UT 84322

Abstract

Lidar (LIght Detection And Ranging) provides the means to quantitatively evaluate the spatial and temporal variability of particulate emissions from agricultural activities, including animal feeding operations. A three-wavelength portable scanning Lidar system built at the Space Dynamic Laboratory (SDL) is used to extract optical properties of the particulate matter from the return Lidar signal and to convert these optical properties to physical parameters including the spatial distribution of particulate concentration around the agricultural facility and its temporal variations. The inversion algorithm developed to retrieve physical parameters of the particulate matter takes advantage of measurements taken simultaneously at three different wavelengths (355, 532, and 1064 nm) and allows us to estimate the particle size distribution in the emitted plume as well; however, quantitative evaluation of particulate optical and physical properties from the Lidar signal is complicated by the complexity of particles composition, particle size distribution, and environmental conditions such as the ambient humidity. Additional independent measurements of particulate physical and chemical properties are needed to unambiguously calibrate and validate the particulate physical properties retrieved from the Lidar measurements. In this paper we present results of the particulate emission characterization obtained by simultaneous remote measurements with Lidar and point measurements at the feeding operation site with standard equipment including optical particle counters, portable PM_{10} and $PM_{2.5}$ ambient air samplers, multistage impactors, an aerosol mass spectrometer, and ion chromatography.

1. Introduction

Agricultural operations produce a variety of particulates and gases that influence ambient air quality and are important to the well-being of humans, animals, and plants. Concentrated Animal Feeding Operations (CAFO) are being investigated by government regulators as one of the major sources of air and water pollutants. The United States Department of Agriculture (USDA) and Agriculture Research Service (ARS) have developed a program to measure the level of pollutants crossing the CAFO boundary and the source and transport phenomenon associated with the pollutant release. The federal government regulations of CAFO are based on point-source pollution measurements located around CAFO facilities. These localized point measurements cannot adequately determine the spatial and temporal distribution of pollutant emission over extended atmospheric regions. Additionally, variations in environmental conditions and pollutant transport activities make it practically and economically infeasible to monitor actual pollutant source strength using point sensors. Lidar (LIght Detection And Ranging) technology (Measures, 1984) provides a means to derive quantitative information of particulate spatial distribution and optical properties over remote distances using one instrument located at a single convenient point. The Space Dynamics Laboratory (SDL) at Utah State University has teamed with ARS researchers to build a Lidar system for remote sensing of pollution from agricultural activities including CAFO. A combination of scanning geometry with a high repetition rate laser allow us to measure representative three dimensional (3D) cross sections of particulate clouds in a reasonable time of a few minutes. For agricultural assessment, the most representative Lidar scan pattern employs repeated vertical scans of the atmosphere on the upwind and downwind sides of a pollutant emission source. When combined with wind speed information, this pattern allows the estimate of source flux rates using the input-minus-output flux difference method (Hipps, 1995). High spatial resolution of 5m and 3D representation of the measured distribution makes the Lidar system a unique instrument for particulate flux measurements and monitoring of flux temporal and spatial variations.

The Lidar technique measures the return signal of laser light scattered by the atmosphere and is equivalent to the integral of the backscatter cross section of the particles (aerosols) present in the atmosphere with the particle size distribution as the weighting function. The aerosol backscatter cross section is uniquely determined by the physical and chemical properties of the aerosols (size, shape, and complex refractive index) and the laser wavelength. The wavelength dependence on the backscatter coefficient is mainly determined by the aerosol size distribution and refractive index. Different aerosol types have different refractive indices and size distributions, which implies that it is possible to discriminate aerosol types according to the wavelength dependence measured by a multiple wavelength Lidar. Using backscatter coefficients measured at several laser wavelengths, the physical properties of aerosols, including size distribution and particle concentration, can be retrieved by determining a solution to the Mie integral equations describing scattering properties of the aerosol (Bockmann, 2001). Thus a multiwavelength Lidar system can provide not only information on the 3D distribution of particulate matter but also information on the particulate size distribution in a 3D space with the ability to convert this information to the standard EPA (Environmental Protection Agency) mass concentration units like PM_{10}, $PM_{2.5}$, and $PM_{1.0}$.

Aerosol sounding techniques for the retrieval of physical aerosol parameters from multi-wavelength Lidar measurements have been developed since the 1980s and have made major progress in the past five years (Heintzenberg et al., 1981; Rajeev et al., 1998; Muller et al., 1999; Bockmann, 2001; Veselovskii et al., 2004). Unambiguous and stable retrieval of aerosol physical parameters requires measurements of backscatter coefficients at least at three laser wavelengths and aerosol extinction coefficients at least at two different wavelengths using additional Raman channels (Althausen et al., 2000; Bockmann, 2001). However, from the instrumental point of view, multi-wavelength Lidar systems with additional Raman channels are still very expensive and complicated to operate. Moreover, Raman signals are comparably weak and require significant integration time to achieve a reasonable signal to noise ratio to be useful for the retrievals (around 30-60 minutes for one measurement (Althausen et al., 2000)). Because of this, most Lidar systems with Raman channels typically operate at night to reduce background radiation from the atmosphere. For agricultural applications we need an inexpensive, robust and easily operated system that is able to provide particulate emission measurements in a matter of a few seconds under any meteorological and diurnal conditions and still be able to distinguish between different types of particulate emissions. A three-wavelength Lidar system appears to be a reasonable tradeoff between accuracy and stability of retrievals while providing the ability to operate under different environmental conditions with minimal measurement time. To date, a significant database of atmospheric aerosol characteristics has been obtained using a combination of satellite and ground based observations (Hess, 1998; Dubovik et al., 2002). Using this database, several researchers have shown that the physical properties of assumed aerosols can be successfully retrieved based on measurements of backscatter coefficients at only three wavelengths (Sasano et al., 1989; Rajeev et al., 1998; Del Guasta et al., 1994).

In this paper we present the initial results of the particulate emission characterization obtained by simultaneous remote measurements with a 3-wavelength Lidar system and in-situ point particulate measurements performed with standard EPA approved equipment. The combination of in-situ and remote measurements with the Lidar system pursues a twofold goal. First, particulate chemical and physical parameters measured in situ are used to make assumptions on the complex refractive index and type/shape of particle size distribution of particulate emissions present on the experiment site. In-situ measurements are also used to constrain the inverse solution to minimize overall errors and uncertainties in the Lidar measurements and the data analysis process. Second, in-situ measurements are used to calibrate and verify the results of Lidar retrievals. The experiment was conducted at the deep-pit swine production facility situated near Ames, in central Iowa, for approximately three weeks during August and September of 2005. An integrated system to measure whole facility emission was designed to characterize the complex structure and temporal/spatial variations in the particulate emission rates often associated with production operations (Bingham et al., 2006).

2. Experiment Setup and Overview of Employed Instrumentation

A schematic diagram of the deep-pit swine production facility and instrumentation employed on this site are shown in Figure 1.
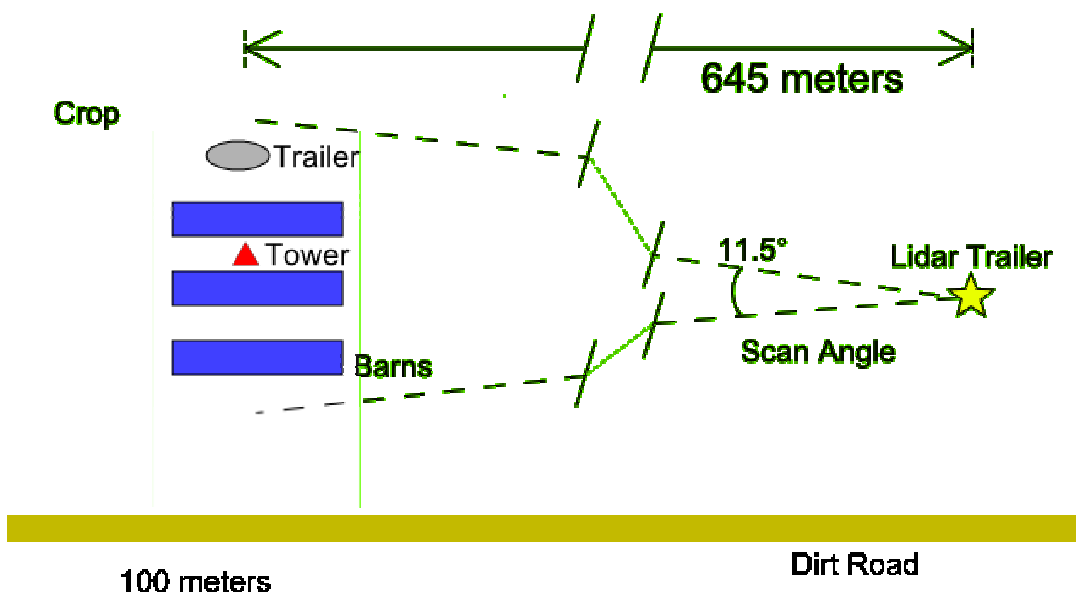
Figure 1. Experimental site layout showing locations of in-situ sensors and the Lidar system

The facility consisted of three separate, parallel barns, each of which housed around 1,250 pigs. The area around the facility was topographically flat and surrounded by fields of soybean and corn. A number of MetOne Optical Particle Counters (OPCs) 9722 were employed around this hog facility with units mounted at various heights on a tower erected at the center of the facility and a point source sensor trailer to provide information on particle size distribution continuously in real time. OPCs have the ability to count airborne particles in eight size ranges from 0.3 to 10 μm in diameter, with sampling time of 20 sec. A pair of Tisch Cascade impactors at the central tower and sensor trailer provided filter-based particle size fractionation and concentration measurements in a range of 0.37-9 μm. To measure chemical composition, real time particle ionic composition, and fine particle size distribution, the Aerodyne Aerosol Mass spectrometer (AMS) was deployed at the trailer. Portable $PM_{10}/PM_{2.5}$ (AirMetrics MiniVol) samplers and passive NH_3 (Ogawa Model 3300) samplers were arrayed vertically and horizontally around the three-barn production facility, and data were collected on a daily-averaged basis. The AirMetrics samplers were operated with $PM_{2.5}$ impactor separation heads for approximately the first half of the field study and were than switched to the PM_{10} heads for the remaining portion of the study. A monitoring Davis weather station was established approximately 40 m to the north of the nearest barn to record the typical suite of meteorological parameters (wind speed, direction, temperature, etc.) for determination of near-source atmospheric advection and dispersion. A detailed description of the instrumentation and results of the in-situ measurements of particulate and gas emission are reported by Martin et al. in the proceedings of this Workshop.

The AGLITE Lidar instrument used in this study is a three-wavelength lidar system being designed and constructed at SDL under a contract with the ARS. A single diode-pumped Nd:YAG laser operating simultaneously at fundamental (IR-near infrared 1.064 μm), doubled (V-visible 0.532 μm), and tripled (UV-near ultraviolet 0.355 μm) frequencies is used as a transmitter of short impulses of radiation to probe scattering particles in the atmosphere. The high repetition rate of 10 kHz allows the use of low pulse energy for eye safe operations at the close ranges required for agriculture applications. The laser beam diameter is 10 mm, and beam divergence is approximately 0.2-0.3 mrad after beam-expanding optics. Outgoing laser energy is monitored by photo-sensors, and this information is transmitted to the data processing unit. The laser light backscattered from particles in the atmosphere is directed by a scanning mirror to a Newtonian telescope with a main-mirror diameter of 28 cm and a field of view (FOV) of 0.46 mrad. The beam-separation unit is used to split up the return backscattered light at three different channels according to wavelength. A photon counting detection system is chosen to detect low return signal simultaneously on

each channel. Interference filters are placed in front of each detector to suppress background daylight radiation from the atmosphere and optical cross talk between channels. The data from the photon counting unit are read out by a digital processing unit, averaged across a predetermined set of laser pulses, displayed in a real time, and stored and/or transmitted for further processing. The whole Lidar system was optimized for eye safe operation at all three wavelengths to allow full daylight operations at ranges from 0.5 to 15 km with a minimal range resolution of 5 m. Technical details of the Lidar design and construction are described by Wilkerson et al. in the proceedings of this Workshop.

The AGLITE Lidar system is trailer-mounted, and the scanning mirror is elevated above the trailer roof to provide a 270^0 azimuth by 45^0 elevation field of measurement. A digital camera co-aligned with the field of view of the Lidar and capturing imagery of the down-range scene is also mounted on the beam director. The AGLITE electronic control system automatically coordinates and synchronizes all the functions of the Lidar, scanning turret, data acquisition system, digital camera, and weather station to provide a complete data package and makes it available to the operator for further analysis. The Lidar trailer was placed at approximately 650 m east of the central tower (see Figure 1) and accompanied by a second weather station to monitor atmospheric conditions near the Lidar. This location of the Lidar system allowed full 3D volume measurements of particulate emissions from the three-barn feeding operations from a single observation point. Typical settings for the Lidar during operation are the following: accumulation time for return signal of 0.5-3 sec per measurement (5,000-30,000 laser pulses), range resolution of 5-15 m at ranges of 0.5-15 km, and azimuth and elevation scan speed of 0.05-2.0°/sec.

3. Inversion of the Lidar Signal to Retrieve Optical and Physical Properties of Aerosols

The Lidar return power from range R for two distinct classes of scatters may be written in the following form (Measures, 1984; Klett, 1985):

$$P(R, \lambda) = C \cdot \frac{P_0(\lambda)}{R^2} \cdot T^2(R, \lambda) \cdot \left[\beta_b(\lambda, R) + \beta_a(\lambda, R) \right] \qquad (1)$$

Where C= $\xi(R, \lambda) \cdot A_0 \cdot \Delta R = \xi(R, \lambda) \cdot A_0 \cdot \tau_d \cdot c/2$ is the Lidar calibration constant that includes losses in the transmitting and receiving optics $\xi(R, \lambda)$ (Lidar overlap geometrical form factor), the effective telescope area A_0, and range increment ΔR acquired by the Lidar that is defined by the detector integration pulse width τ_d and speed of light c. $P_0(\lambda)$ is a total laser power transmitted at wavelength λ. $\beta_b(\lambda, R)$ and $\beta_a(\lambda, R)$ stand for the backscatter coefficients of air molecules and aerosol particles, respectively. Round trip laser beam transmittance along the beam pass $T^2(R, \lambda)$ is defined by the equation:

$$T^2(R, \lambda) = \exp \left\{ -2 \int_0^R [\alpha_b(\lambda, R') + \alpha_a(\lambda, R')] \partial R' \right\} \qquad (2)$$

Where $\alpha_b(\lambda, R)$ and $\alpha_a(\lambda, R)$ are extinction coefficients of air molecules and aerosols, respectively.

Retrieval of aerosol physical parameters from a raw Lidar signal involves four major steps:

1) Account for geometrical form factor of the telescope receiving optics and scattered sunlight background radiation. The geometrical form factor in equation (1) takes into account the overlap between the transmitted laser beam and the FOV of the telescope receiving optics with the central obstruction and can be estimated theoretically (Measures, 1984). In real life, this factor can change after setup of the portable Lidar system in the field, and the real geometrical form factor $\xi(R, \lambda)$ shall be determined experimentally. To calculate the geometrical form factor at field conditions, the polynomial regression method for an inhomogeneous atmosphere proposed by Dho et al., 1997 is used. This method does not require special atmospheric conditions and in many cases can be used during operational field measurements. During daylight observations the background radiation of sunlight scattered by the atmosphere dominates the Lidar return signal at long distances. For each Lidar measurement this background radiation is approximated by least

squares fitting to a constant value at distances of 13-15 km and then subtracted from the total Lidar return signal.

2) Calculate the optical parameters (backscatter and extinction coefficients) of the background aerosols and particulate emission from the feeding facility at three wavelengths, utilizing Klett's analytical solution for two scattering components (Klett, 1985). Typically, the molecular part of equation (1) can be calculated using standard atmosphere conditions at different altitudes and the well known and parameterized refractive index, backscatter and extinction properties of the air molecules (Bockmann, 2004). Aerosol backscatter and extinction coefficients remain two unknowns in a single Lidar equation that describes one particular Lidar measurement. We are using the standard solution of this equation proposed by Klett that involves a priori assumption of the relationship between aerosol extinction and backscatter coefficients that is usually called the Lidar ratio L:

$$L_a = \alpha_a(\lambda, R) / \beta_a(\lambda, R) \tag{3}$$

Another assumption deals with selecting a boundary value to determine the constraint factor required by Klett's solution, usually a calibration or reference value of the extinction coefficient $\alpha_{aD} = \alpha_{aD}(\lambda, R_D)$ independently measured at a certain distance R_D.

The original solution of equation (1) has been deducted for typical atmospheric applications when the Lidar system is looking straight up so that molecular contribution is significant for altitudes above the aerosol boundary layer (ABL). For agricultural applications all measurements are conducted close to the ground, and the main contribution to atmospheric scattering is determined by aerosols while the molecular contribution is negligibly small. In this case we are still dealing with two distinct types of scatterers such as background aerosols and airborne particulate matter emitted from the agricultural activities. For this application, the original solution of equation (1) is still valid, and we attribute the subscript "b" to the atmospheric background aerosols while the subscript "a" will refer to the particulate emission. Typically the agricultural particulate emission is spatially localized around the emission source while the rest of the Lidar signal is dominated by the surrounding background aerosols. In close proximity to the emission source the background aerosol loading is typically homogeneous, and a standard slope method (see for instance Klett, 1985) can be applied to retrieve the extinction coefficient of the background aerosols. For each wavelength, the slope of a line that has been fit in a least-squares sense to the curve S(R) is used as an estimate of $\alpha_b(\lambda, R)$ over the interval where $S(\lambda, R) = \ln[P(R, \lambda) \cdot R^2]$ presents nearly a straight line.

3) Estimate parameters of particle size distribution for background aerosols and particulate emission using an iterative technique to minimize the difference between simulated (Mie theory) and measured extinction coefficients at three Lidar wavelengths.

Based on the OPC data measured in situ, we approximate the particle size distribution by a bimodal distribution, using the standard Power low function for the accumulation mode:

$$n(r) = N_1 r^\nu \tag{4}$$

and lognormal size distribution for the coarse particle mode:

$$n(r) = \frac{1}{r} \frac{N_2}{(2\pi)^{1/2} \cdot \ln\sigma} \cdot \exp[\frac{(\ln r - \lg r_m)^2}{2 \cdot \ln^2 \sigma}] \tag{5}$$

Where N_1 is a constant related to the total number of particles with radius r in accumulation mode and ν is the size index that generally varies in a range of 3-5. N_2 represent the total density of particles in the coarse mode with mode radius of r_m and width of distribution σ.

To estimate the mode radius and particle number densities N_1 and N_2, we are using a modified version of the minimization technique described by Del Guasta (1994). The minimization function in our case is constructed on the differences between the extinction coefficients α_i, retrieved from the Lidar signal, and α_i^{calc}, calculated using Mie theory (Bockman, 2001) at three laser wavelengths. Arbitrary values of the Lidar ratio for both background aerosols L_b and particulate

emission L_a are assumed initially at step 2. Estimated particle size distributions in step 3 are used to update these values through Mie calculations. Steps 2 and 3 are then repeated iteratively to achieve a minimal value of the minimization function.

4) Calculate volume concentration and convert it to the mass concentration using in-situ chemical and physical property measurements. Once the parameters of particle size distribution and number densities are estimated, the mass concentration of particles with different size ranges can be easily calculated using in-situ measurements of particulate chemical composition and density (Hinds, 1998).

4. Experimental Results and Discussion

An extended series of Lidar observations were conducted during three weeks of field campaign at the deep-pit swine production facility. Most of measurements were conducted at day and night time to capture the dynamic of particulate flux emission from the production facility. The local climate was typically characterized by clear skies, and winds were generally mild at 0-3 m/s, changing direction from west to south during the study period. Typical Lidar scan patterns include vertical scans between barns and on any side of the barns and sensor trailer, horizontal scans above the barns at any chosen elevation, stationary time series scans of particulate emission in close proximity to the in-situ instrumentation, and any combination of vertical and horizontal scans to capture and monitor 3D distribution and variation of the particulate emission. Depending on the prevailing wind conditions, the measured profiles of particulate emission varied significantly from day to day and occasionally even hour to hour.
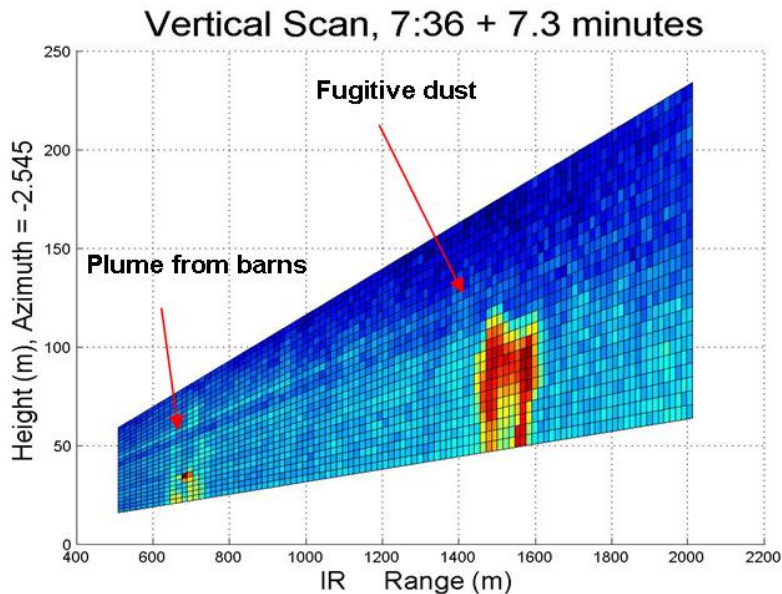

Figure 2. Vertical Lidar scan measured at λ=1.064 µm near the central tower on 09/02/05, 7:36 am under still weather conditions
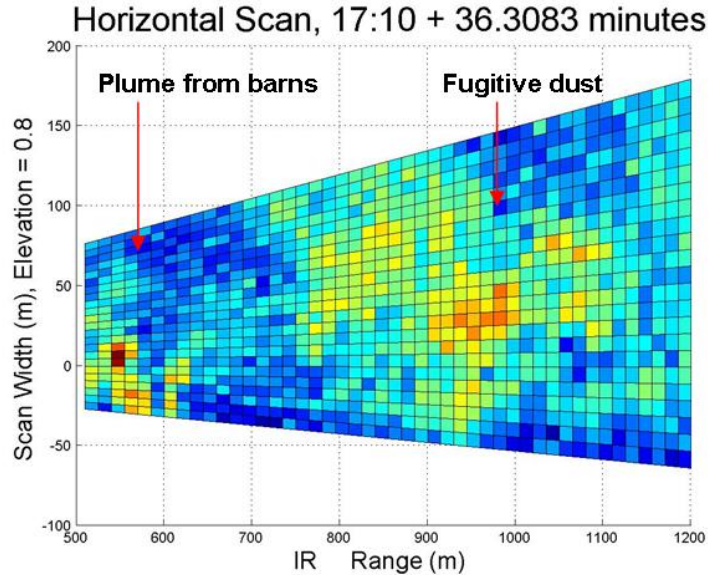
Figure 3. Horizontal Lidar scan measured at λ=1.064 μm on the elevation of ~5m above the barns on 09/01/05, 5:10 pm under west wind of 3 m/s.
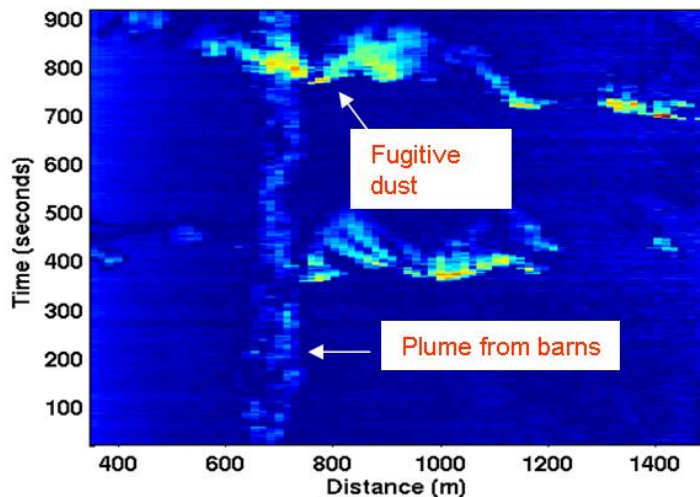
Figure 4. Time series of pollutant and fugitive dust emissions measured at λ=1.064 μm under south wind conditions when Lidar is pointing at the middle of the tower.

Two dirt roads were bordering the swine production facility. One road ran east to west at a distance of ~115 m south from the central measurement tower. The second road ran north to south at a distance of ~900 m west from the tower. Occasional traffic along both roads caused extensive fugitive dust traveling from roads over the swine facility. These events were captured as well during Lidar operations. Examples of vertical, horizontal, and pointed (time series) Lidar scans are shown in Figures 2, 3, and 4 respectively.

These images are rendered in false color where the color represents the intensity of semi-processed Lidar return signals with background radiation from the sun and background aerosols removed. In all images the particulate emission from the barns is clearly distinguished from the fugitive road dust due to separation of these events in space and time. The particulate emission from barns was localized between barns at a distance of ~650 m from the Lidar (the location of the central measurement tower), while fugitive dust clouds (Figures 2 and 3) were coming from the western road located at a distance of ~1550 m from the Lidar. The vertical scan in Figure 2 was measured at a still wind condition so that both the fugitive dust cloud and the particulate emission were spatially localized around the emission sources expanding upward

due to convective turbulence. The horizontal scan in Figure 3 was taken under west wind conditions, and the data show that both particulate emission and fugitive dust were swept by the wind toward the Lidar and extended horizontally as compared to Figure 2. The time series in Figure 4 was measured under south wind conditions when fugitive dust was blown from the south road, which was parallel to the line of Lidar range measurements. A weaker signal at a range of ~650 m represents particulate emission between swine barns measured at a height of ~6 m in a close proximity to the OPC sensor mounted on the tower.

Due to the spatial and temporal separation of different particulate emissions in the return Lidar signal, these events can be easily processed separately so that optical and physical properties of particulate emissions from different sources can be extracted using single Lidar scan. For all cases the return signals from fugitive dust clouds were about an order of magnitude stronger than the signal from barn particulate emissions, which in some cases only slightly exceeded Lidar returns from the background aerosols in the air surrounding the facility. The retrieval procedure briefly described in a previous section was tested on both cases, for which there are remarkably different physical origins of particulate emissions involved.

Proper conversion of Lidar data involves the construction of a model for the particulate composition and size distribution based on in-situ measurements. Following the OPAC database (Hess, 1998) we assumed that fugitive dust is composed of a mixture of quartz and clay materials. Particle size distribution was approximated by a bimodal distribution based on in-situ measurements with OPC sensors. The results of the retrievals are shown in Figure 5. Extinction coefficients retrieved at three laser wavelengths in step 2 are shown in Figure5A as a function of the distance from Lidar. The dust cloud chosen for conversion is extended for almost 1km from the west road toward Lidar and shows different ratio of extinction coefficients measured at different wavelengths. As a result, the parameters of particle size distributions estimated at different distances are different, which leads to a different ratio of small (accumulation mode) and large (coarse mode) particles within the same dust cloud.
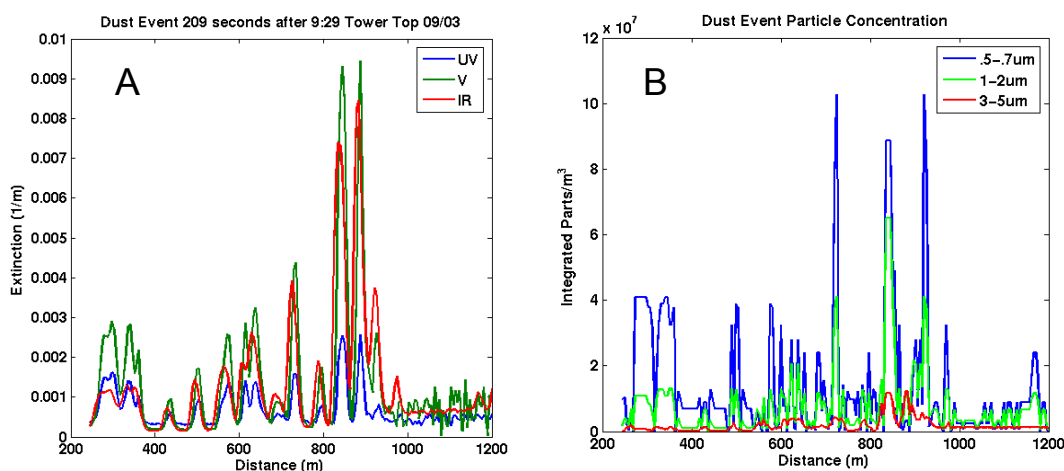

Figure 5. Optical and physical properties of fugitive dust cloud retrieved from the Lidar signal at different distances from the Lidar. A) Extinction coefficient at three Lidar wavelengths. B) Volume concentrations for dust particles with radius range of 0.5-0.7 μm, 1-2μm, and 3-5 μm estimated from extinction coefficients.
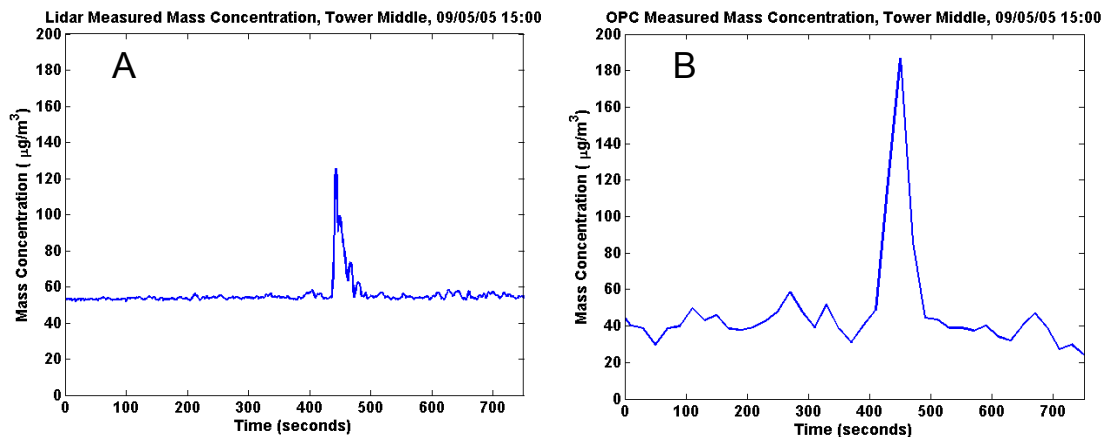
Figure 6. Time series of dust particles mass concentration PM$_{10}$ as measured by the Lidar (graph A) and OPC sensor mounted on the top of the tower (graph B). Measurements are collocated in time and space.

Volume concentrations of particles with radiuses in a range of 0.5-0.7 µm, 1-2 µm, and 3-5 µm were calculated from size distributions estimated in the retrieval step 3 and are shown in Figure 5B. It is seen that the large particle concentration decreases while the concentration of small particles increases with the distance from road along the wind, showing settlement of large particles from the dust cloud.

Mass concentration PM$_{10}$ estimated from the Lidar signal is compared with in-situ measurements by OPC in Figure 6. Both measurements represent a time series of particulate emission measured simultaneously at the top of the tower, where the peak concentration represents a fugitive dust event and the base signal is mostly due to the background aerosols. Concentration of background aerosols and fugitive dust from the road measured by the Lidar are both in good quantitative agreement with coincident OPC measurements.

As mentioned previously, particulate emissions from the swine facility only slightly exceed the background aerosol loading. Lidar returns are still sensitive to these small variations, which can be easily spotted due to their spatial localization in the return Lidar signal. The OPC sensors provide continuous point measurements so that background aerosols and particulate emission can be distinguished only by the numbers of counts (intensity of the signal). Comparison of the OPC data measured between barns and far away from barns where only background aerosol is present shows that particulate emission counts are on the level of natural variability of the background aerosol loading. In this case it is difficult to extract exact information on the particulate size distribution from the OPC data. Taking this into account, we also approximated the particulate size distribution by a bimodal distribution, as in a case of fugitive dust and background aerosols. Preliminary chemical analysis of the particulate emission measured in situ (Martin, 2006) shows that its composition may be considered as a standard water soluble aerosol mixture composed from various kind of sulfates, nitrates, organic carbon, etc. (Hess, 1998). Assuming these approximations, Lidar returns from a particulate plume were processed and parameters of particulate size distribution were estimated as described in section 3. Once parameters of particle size distribution are estimated, the mass concentration of PM$_{2.5}$ is calculated assuming an average particle density of 1.8 g/cm^3. The results of these calculations are shown in Figure 7 for two time series of Lidar measurements pointed at the middle of the tower and at its top.
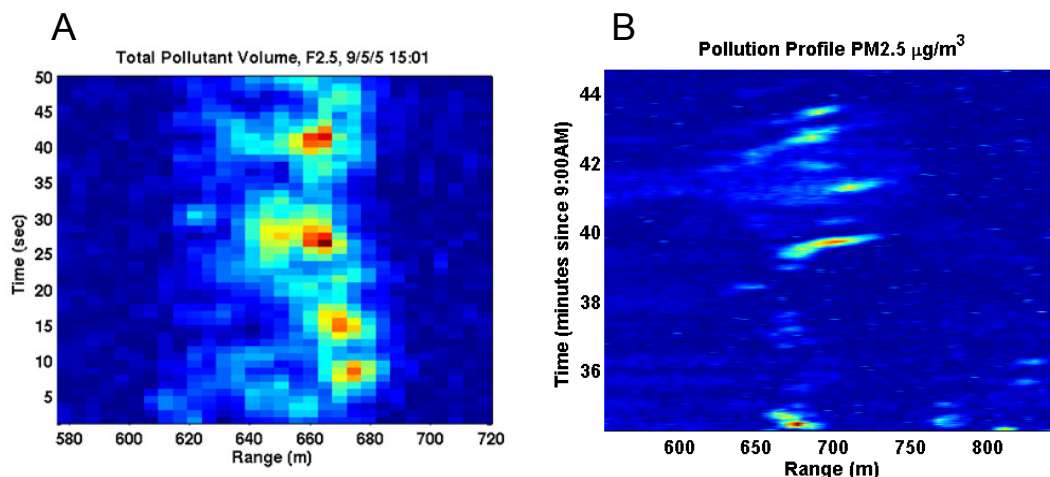
A

Total Pollutant Volume, F2.5, 9/5/5 15:01

B

Pollution Profile PM2.5 $\mu g/m^3$

Figure 7. Comparison of the PM10 concentration at the middle of the tower (A) and at the tower top (B) as estimated from the Lidar returns.

It interesting to note that particulate was emitting from barns as periodical events with periodicity of 3-10 seconds as can be seen in both images of Figure 7. During these observations the Lidar accumulation time was set to 1 second, and that was enough to resolve the periodic nature of particulate emission. The accumulation time of OPC monitoring sensors was 20 seconds so that OPC counts represent a time average of periodic events that contributed to the inability of OPC sensors to resolve clearly particulate emissions and background aerosols.

Preliminary comparisons of the Lidar retrievals with in-situ $PM_{2.5}$ measurements shows that total $PM_{2.5}$ mass concentration agrees within an order of magnitude.

5. Conclusion

A three-wavelength portable scanning Lidar system has been developed at SDL to derive information of particulate spatial distribution and optical/physical properties of aerosols over remote distances using an instrument located at a single convenient point. Preliminary results discussed in this paper show the great potential of remote Lidar measurements to quantitatively characterize particulate emission from different sources. Lidar technology represents a unique technique to characterize spatial and temporal variations of particulate emission from any source met in field conditions. Additionally, the high measurement rate of the Lidar allows us to capture temporal variations in particulate emissions on the order of seconds that could not be resolved by most in-situ point instrumentation. The use of extinction/backscatter ratios derived from Lidar measurements at three laser wavelengths was found to be a promising method for remote measurements of the size distribution of particulate emissions present in the field. These emissions include background aerosols, emissions from the feeding facility, and fugitive dust from the road. The strength of Lidar returns from these sources varies by an order of magnitude, and the inversion algorithm developed to process three wavelengths Lidar data gives meaningful results for all sources of particulate emissions. Retrieval results for fugitive road dust are in a good agreement with coincident in-situ measurements by OPC sensors. The retrievals of mass concentration of particulate emission from the feeding operation agree on the order of magnitude with in-situ measurements performed with $PM_{2.5}$ ambient samplers. The main uncertainties involved in such a method are due to the incomplete knowledge of the particulate refractive index and parameters of particle size distribution to further constrain the iterative minimization technique employed in this method to estimate parameters of assumed size distribution. Further work is needed for both remote Lidar and in-situ point measurements to verify, calibrate, and correlate all types of measurements performed in the field.

References

Althausen D., D. Muller, A. Ansmann, U. Wandinger, H. Hube, E. Clauder, and S. Zorner. 2000. Scanning six-wavelength eleven channel aerosol lidar. *J. Atmos. Ocean. Technol.* 17: 1469–1482.

Bingham G. E., J. Hatfield, J. H. Prueger, T. D. Wilkerson, V. V. Zavyalov, R. L. Pfeiffer, L. Hipps, R. Martin, P. Silva, W. Eichinger. 2006. An Integrated Approach to Measuring Emissions from Confined Animal Feeding Operations at the Whole Facility Scale. Proceedings of the Workshop on Agricultural Air Quality: June 5-8.

Bockmann C. 2001. Hybrid regularization method for ill-posed inversion of multiwavelength lidar data in the retrieval of aerosol size distributions. *Appl. Opt.* 40: 1329–1342.

Bockmann C. , U. Wandinger, A. Ansmann, J. Bosenberg, V. Amiridis, A. Boselli, A. Delaval, F. De Tomasi, M. Frioud, I.V. Grigorov, A. Hagard, M. Horvat, M. Iarlori, L. Komguem, S. Kreipl, G. Larcheveque, V. Matthias, A. Papayannis, G. Pappalardo, F. Rocadenbosch, J. A. Rodrigues, J. Schneider, V. Shcherbakov, and M. Wiegner. 2004. Aerosol lidar intercomparison in the framework of the EARLINET project. 2. Aerosol backscatter algorithms. *Appl. Opt.* 43: 977-989.

Del Guasta M., M. Morandi, L. Stefanutti, B. Stein, and J. P. Wolf. 1994. Derivation of Mount Pinatubo stratospheric aerosol mean size distribution by means of a multiwavelength lidar. *Appl. Opt.* 33: 5690–5697.

Dho S. W., Y. J. Park, and H. J. Kong, 1997. Experimental determination of a geometrical form factor in a lidar equation for an inhomogeneous atmosphere. *Appl. Opt.* 36: 6009-6010.

Dubovik O., B. Holben, T. F. Eck, A. Smirnov, Y. J. Kaufman, M. D. King, D. Kino, D. Tanre, and I. Slutsker. 2002. Variability of absorption and optical properties of key aerosol types observed in worldwide locations. *J. Atm. Scie.* 59: 590-608.

Heintzenberg J., H. Muller, H. Quenzel, and E. Thomalla. 1981. Information content of optical data with respect to aerosol properties: numerical studies with a randomized minimization-search-technique inversion algorithm. *Appl. Opt.* 20: 1308–1315.

Hess M., P. Koepke, and I. Schult. 1998. Optical Properties of Aerosols and Clouds: The software package OPAC. *Bull. Am. Meteorol. Soc.* 79: 831-844.

Hinds W. C. 1998. *Aerosol technology. Properties, behavior, and measurement of airborne particles.* John Willey & Sons, Inc., New York.

Hipps L.E. and D.F. Zehr. 1995. Determination of evaporation from integrated profiles of humidity and temperature over an inhomogeneous surface. *Boundary-Layer Meteorol.* 75: 287- 299.

Klett J. D. 1985. Lidar inversion with variable backscatter/extinction ratio. *Appl. Opt.* 24: 1638-1683.

Martin R.S., V. Doshi, and K. Moore. 2006. Determination of Particle (PM10 and PM2.5) and Gas-Phase Ammonia (NH3) Emissions from a Deep-Pit Swine Operation using Arrayed Field Measurements and Inverse Gaussian Plume Modeling. Proceedings of the Workshop on Agricultural Air Quality: June 5-8.

Measures R. M. 1984. *Laser remote sensing: Fundamentals and applications.* John Willey & Sons, Inc., New York.

Muller D., U. Wandinger, and A. Ansmann. 1999. Microphysical particle parameters from extinction and backscatter lidar data by inversion with regularization: theory. *Appl. Opt.* 38: 2346–2357.

Rajeev K. and K. Parameswaran. 1998. Iterative method for the inversion of multiwavelength lidar signals to determine aerosol size distribution. *Appl. Opt.* 37: 4690–4700.

Sasano Y. and E. V. Browell. 1989. Light scattering characteristics of various aerosol types derived from multiple wavelength lidar observations. *Appl. Opt.* 28**:** 1670-1679.

Veselovskii I., A. Kolgotin, V. Griaznov, D. Muller, K. Franke, and D. N. Whiteman 2004. Inversion of multiwavelength Raman lidar data for retrieval of bimodal aerosol size distribution. *Appl. Opt.* 43: 1180-1195.

Wilkerson T.D., G. E. Bingham, V. V. Zavyalov, J. A. Swasey, J. J. Hancock, B. G. Crowther, S. S. Cornelsen, C. Marchant, J. N. Cutts, D. C. Huish, C. L. Earl, J. M. Andersen, and M. L. Cox. 2006. AGLITE: A Multiwavelength Lidar for Aerosol Size Distributions, Flux and Concentrations of Whole Facility Emissions. Proceedings of the Workshop on Agricultural Air Quality: June 5-8.